Dalton Transactions

Accepted Manuscript

ROYAL SOCIETY OF CHEMISTRY

www.rsc.org/dalton

Table of Content

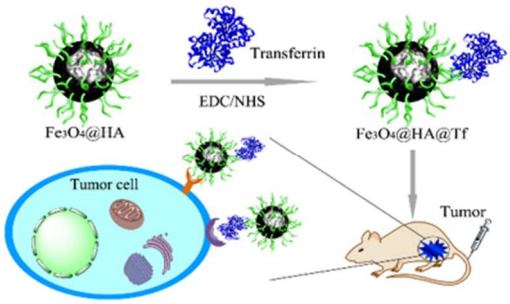

A biocompatible and sensitive dual-targeting Fe_3O_4 nanoprobe co-modified with biosafe hyaluronic acid and transferrin was developed for tumor-targeted MR imaging.

Journal Name

PAPER

Facile preparation of hyaluronic acid and transferrin co-modified Fe_3O_4 nanoparticles with inherent biocompatibility for dual-targeting magnetic resonance imaging of tumors *in vivo*

Received 00th January 20xx,
Accepted 00th January 20xx

DOI: 10.1039/x0xx00000x

www.rsc.org/

Jinbin Pan,‡[a] Shao-Kai Sun,‡[b] Yaqiong Wang,[b] Yan-Yan Fu,[b] Xuejun Zhang,[b] Yi Zhang[c] and Chunshui Yu*[a]

Clinical diagnosis of malignant tumors using nanoprobes needs severe acquirement in the aspects of sensitivity and biocompatibility. Integrating dual-targeting strategy and selection of human-inherent elements and molecules as raw materials shows great potential in the development of biosafe and sensitive nanoplatform. To carry out the proposed design, we constructed a biocompatible dual-targeting MR imaging nanoprobe based on Fe_3O_4 nanoparticles (NPs) co-modified with inherently innoxious hyaluronic acid (HA) and transferrin (Tf). HA was used as both the template and targeting molecule to form the Fe_3O_4@HA NPs through a one-step co-precipitation method, which were further modified with Tf to obtain the dual-targeting Fe_3O_4@HA@Tf NPs at room temperature. The excellent biocompatibility of the nanoprobe was demonstrated via toxicity assays *in vitro* and *in vivo*. The desirable dual-targeting ability to tumor cells was confirmed by the cellular (Hela cells, overexpressing both CD44 and transferrin receptors) uptake test, and the developed nanoprobe was successfully applied in tumor-targeted MR imaging *in vivo*. In a word, we developed a dual-targeting Fe_3O_4 nanoprobe with high targeting ability to tumor cells and excellent biocompatibility following a facile procedure at room temperature, which enjoyed great potential in the application of clinical diagnosis of tumors.

1. Introduction

Early diagnosis of malignant tumors plays a crucial role in extending the survival period of patients followed by the standardized clinical treatments.[1] To achieve this significant goal, several tumor targeting strategies based on the nanotechnology have been developed, such as passive tumor targeting via the enhanced permeability and retention (EPR) effect,[2, 3] active tumor targeting guided by single-[4-7] or dual-targeting ligands,[8-10] and smart probes responded to the special microenviroment (pH, temperature and enzyme) of tumor cells.[11, 12] Among these strategies, dual-targeting modification has obtained an increasing attention to researchers due to its high targeting ability via synergistic targeting effect to tumor cells.[13] Although outstanding advantages of dual-targeting strategy were universally recognized, the previous routines for building a dual-targeting nanoplatform suffered from tedious synthesis procedures and tough reaction conditions, which potentially influenced the activity of targeting molecules. So contriving a new dual-targeting nanoplatform with a facile synthesis procedure under mild conditions is in high demand.

Biocompatibility, an unavoidable challenge in the probable clinical applications of various nanoprobes, seriously hinders plenty of nanoprobes with excellent targeting imaging ability in the further achievement towards clinical translational medicine.[14-17] Even appropriate physicochemical features, efficient targeting ability and promising theranostic effects of certain nanoparticles have been exhibited *in vitro* and *in vivo*, ambiguous metabolism manners, potential systemic toxicity and larvaceous biochemical influences are still questioned.[18-22] As a result, few nanoprobes like Fe_3O_4 nanoparticles (NPs) has actually been applied to clinical diagnosis, but with hardly satisfactory targeting ability to tumors. As just mentioned, Fe_3O_4 as a T_2-weighted imaging contrast agent in magnetic resonance (MR) imaging,[23-25] has been deeply investigated in the aspects of metabolism and biotoxicity.[26-28] After intravenous administration of Fe_3O_4 NPs *in vivo*, the nanoparticles are phagocytized by the cells and subsequently metabolized in the lysosomal compartment to be the free iron, which will be utilized to compose the iron stores of body.[29] Hence, it is highly attractive to develop a dual-targeting nanoplatform based on biocompatible Fe_3O_4 NPs, which possesses excellent tumor targeting ability and admirable biosafety in a relatively facile procedure.

[a] Department of Radiology, Tianjin Key Laboratory of Functional Imaging, Tianjin Medical University General Hospital, Tianjin 300052, China. Email: chunshuiyu@tijmu.edu.cn
[b] School of Medical Imaging, Tianjin Medical University, Tianjin 300203, China
[c] Department of Medical Chemistry, Tianjin Key Laboratory on Technologies Enabling Development of Clinical Therapeutics and Diagnostics (Theranostics), College of Pharmacy, Tianjin Medical University, Tianjin 300070, China
‡These authors contributed equally to this work.
†Electronic Supplementary Information (ESI) available: FT-IR spectra, UV-vis-NIR absorption spectra, size distribution, metabolic result, MR signal change of tumor site and body weight change of mice. See DOI: 10.1039/x0xx00000x

To meet the severe acquirement in the aspects of biocompatibility in clinical medicine, the selection of human-inherent targeting ligands with undoubted inherent biosafety is a charming strategy to further improve the biocompatibility of nanoprobes.[30-32] Hyaluronic acid (HA) is an essential glycosaminoglycan in human body from the extracellular matrix to the corpus vitreum. Due to its special binding with CD44 overexpressed in many malignant tumor cells, it is also extensively employed in tumor-targeted imaging and drug delivery.[30, 31, 33, 34] Another candidate grabbing our attention is transferrin (Tf), a single-chain glycoprotein, which is also the iron containing protein mainly in plasma and responsible for transferring iron ions absorbed by digestive tubes and released from degraded red cells. It is likewise known to be an impactful targeting biomolecule to the transferrin receptors (TfR) overexpressed in many tumor cells.[32, 35] Apparently, both HA and Tf are ubiquitous in human body, which shows undoubted inherent biocompatibility compared with other ectogenic molecules. Herein, we attempt to construct a novel Fe_3O_4 nanoprobe co-modified with HA and Tf in a facile procedure, which possesses high targeting ability and excellent biocompatibility for MR imaging of tumors.

In current work, we synthesized Fe_3O_4@HA NPs using HA as both template and targeting molecules via a one-step co-precipitation method at room temperature. Then the prepared Fe_3O_4@HA NPs were further modified with Tf to generate dual-targeting Fe_3O_4@HA@Tf NPs at room temperature. The biosafety of the proposed Fe_3O_4@HA@Tf NPs was demonstrated *in vitro* and *in vivo* through cell viability assay, intravital metabolism and biochemical analysis respectively. The cellular uptake and blocking tests were performed to study the tumor targeting ability of the developed nanoprobe. Finally, the Fe_3O_4@HA@Tf NPs were successfully applied in tumor-targeted MR imaging *in vivo* (Scheme 1). To our best knowledge, no dual-targeting Fe_3O_4 nanoprobe using human-inherent targeting ligands prepared at room temperature has been reported for targeting MR imaging of tumors so far.

2. Experimental section

2.1 Materials and reagents

All reagents were at least analytical grade. Ultrapure water (Hangzhou Wahaha Group Co. Ltd., Hangzhou, China) was used throughout this work. Hyaluronic acid sodium salt (HA, Mw ≈ 6000) was obtained from Bloomage Freda Biopharm Co. Ltd. (Jinan, China). Iron(III) chloride hexahydrate ($FeCl_3 \cdot 6H_2O$), iron(II) chloride tetrahydrate ($FeCl_2 \cdot 4H_2O$), ammonium hydroxide (NH_4OH), 1-ethyl-3(3-dimethylaminopropyl) carbodiimide (EDC), N-hydroxysuccinimide (NHS), 3-(4,5-Dimethylthiazol-2-yl)-2,5-diphenyltetrazolium bromide (MTT), coomassie brilliant blue G-250, phosphoric acid (85%) were all purchased from Aladdin Reagent Co. Ltd. (Shanghai, China). Human Tf was purchased from Sigma-Aldrich (St. Louis, MO, USA). Poly (ethylene glycol) bis (carboxymethyl) ether (PEG-2COOH, Mw ≈ 2000) was bought from Beijing Kaizheng Biotech (Beijing, China). Ethanol and dimethyl sulfoxide (DMSO) were obtained from Concord Technology (Tianjin, China).

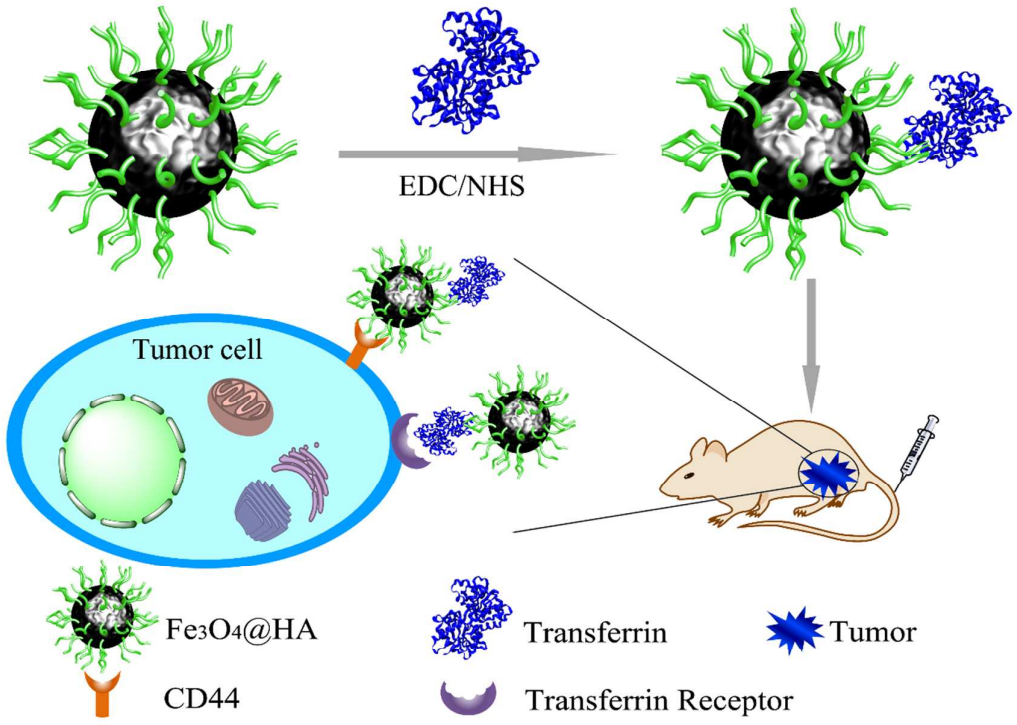

Scheme 1 Schematic illustration of the fabrication of the dual-targeting Fe_3O_4@HA@Tf NPs for tumor-targeted MR imaging

2.2 Characterizations

The content of Fe element in Fe_3O_4@HA@Tf NPs was measured by Atomic Absorption Spectroscopy (AAS, Hitachi 180-80, Japan). The size and morphology of Fe_3O_4@HA@Tf NPs were characterized by high-resolution transmission electron microscopy (HRTEM, Philips Tecnai G^2 F20, Holland). Samples for HRTEM were prepared by coating a dilute nanoparticles suspension into a 230-mesh Cu grid and dried in air before measurements. The X-ray diffraction (XRD) spectra of the nanoparticles were obtained on an X-ray diffractometer (Rigaku D/max-2500, Rigaku, Tokyo, Japan) with Cu Kα radiation. The Fourier transform infrared (FT-IR) spectra of the nanoparticles (of 400-4000 cm^{-1}) were collected with a spectrometer (Nicolet IR AVATAR-360, Nicolet, USA) with pure KBr as the background. UV-vis-NIR absorption spectra was recorded using a U-3900 UV-VIS spectrophotometer (Hitachi, Japan). The thermal gravimetric analysis (TGA) was conducted on a PTC-10A thermal gravimetric analyser (Rigaku, Japan) from room temperature to 800 °C at a ramp rate of 10 °C min^{-1}. The zeta-potential and dynamic light scattering (DLS) of the nanoparticles were measured on a Malvern Zetasizer (Nano series ZS, UK). T_2 relaxivity (r_2) and T_2-weighted MR images of Fe_3O_4@HA@Tf NPs were obtained from a 0.5 T MesoMR60 (Shanghai Niumag Corporation, China) with following parameters: multi spin-echo, TR/TE =2000/60 ms, FOV of 100 ×100 mm, slices=1 and matrix of 192×256. The samples used for evaluation of r_2 were prepared with different Fe concentrations (0, 0.018, 0.036, 0.054, 0.089 and 0.143 mM).

2.3 Preparation of Fe_3O_4@HA NPs and Fe_3O_4@PEG NPs

The Fe_3O_4@HA NPs were prepared via a simple co-precipitation method. Briefly, 0.5 g of $FeCl_3 \cdot 6H_2O$ and 0.184 g of $FeCl_2 \cdot 4H_2O$ were dissolved in 25 mL of ultrapure water in a three-necked flask with vigorous mechanical stirring under the Ar_2 atmosphere for 15 min. Then 7.5 mL of NH_4OH was added to the mixture, and the colour of the solution changed from yellow to black immediately, which indicated the formation of Fe_3O_4 NPs. Subsequently, 5 mL of HA (40 mg/mL) was added to the above solution, then the reaction was proceed for another 30 minutes under vigorous stirring at room temperature. The nanoparticles were collected with the help of an external magnet and washed 3 times with ultrapure water. The Fe_3O_4@PEG NPs were synthesized in the same procedure of Fe_3O_4@HA NPs with only change of replacing HA with PEG-2COOH. The purified Fe_3O_4@HA and Fe_3O_4@PEG NPs were respectively dispersed in 20 mL of ultrapure water and stored at 4 °C for further use.

2.4 Synthesis of Fe_3O_4@HA@Tf NPs

50 mg of Fe_3O_4@HA NPs were dispersed in 20 mL of PBS (pH 7.0) in a round bottom flask, and then 7.2 mg of EDC and 4.3 mg of NHS were added under vigorous mechanical stirring for 1 h. 5 mg of Tf dispersed in 1 mL of PBS (pH 7.0) was added to the solution and stirred for 4 h. Then the formed Fe_3O_4@HA@Tf NPs were washed 3 times with ultrapure water under the help of a magnet to remove the excess reactants. All the supernatant during washing steps was collected and diluted to a final volume of 30 mL with ultrapure water for the use of quantitative analysis of Tf. Finally the purified product redispersed in ultrapure water and the supernatant were stored at 4 °C in dark for further use.

2.5 Cell line experiments

2.5.1. Cell culture. Human cervical carcinoma cell lines（Hela cell, CD44 positive, transferrin receptor positive）were regularly cultured in RPMI-1640 cell medium supplemented with 10% fetal bovine serum (FBS) and 1% streptomycin-penicillin in the atmosphere of 5% CO_2 at 37 °C.

2.5.2. *In vitro* cytotoxicity assay. The MTT assay of Hela cells was carried out to evaluate the cytotoxicity of the Fe_3O_4@HA@Tf NPs *in vitro*. The Hela cells were cultured in a 96-well plate at 8×10^3/well in RPMI-1640 cell medium (200 μL) with 10% FBS and 1% streptomycin-penicillin in the atmosphere of 5% CO_2 at 37 °C for 24 h. Then, the stale medium was replaced with the fresh medium in the presence of different concentrations of nanoprobes (0, 25, 50, 100, 150, 200 and 250 μg/mL) for another 24-hour incubation with 5% CO_2 at 37 °C. Each well was washed with PBS and treated with fresh medium containing 10 μL of MTT (5 mg/mL) and then incubated for an additional 4 h with 5% CO_2 at 37 °C. Then, the medium in each well was replaced by 120 μL DMSO to dissolve the purple formazan crystals. After a 10-minute mild shake, the absorbance values at 490 nm of each well were measured by a microplate reader (Bio-tek).

2.5.3. *In vitro* targeted cellular uptake test. Targeted cellular uptake of Fe_3O_4@HA@Tf NPs by Hela cells was investigated by AAS. Briefly, the Hela cells were cultured in a 24-well plate at 4×10^4/well in RPMI-1640 cell medium (1 mL) with 10% FBS and 5% CO_2 at 37 °C for 24 h. Then, the fresh culture medium was used to replace the stale one. In the meantime, cells in parts of wells were treated with blocking reagents (0.5 mg/mL HA, 0.5 mg/mL Tf, both 0.5 mg/mL HA and Tf, respectively). After 4-hour incubation, the supernatant in each well was removed. The cells were cultured with 1 mL new medium containing Fe_3O_4@HA@Tf NPs at the concentration of 50 μg/mL for another 4 hours. Cells incubated without the nanoparticles were regarded as control. Subsequently, the medium was discarded and each well was rinsed with PBS for 3 times. Then the cells were treated with trypsin and aqua regia (nitric acid/hydrochloric acid, v/v=1:3). Same procedures were performed for the concentration of Fe_3O_4@HA@Tf NPs at 100 μg/mL. At last, all the samples were collected and diluted, and the Fe concentrations in different groups were measured by AAS.

2.6 MR imaging of normal model *in vivo*

In vivo MR imaging of adult kunming mice (25-27 g) purchased from Beijing HFK Bioscience Co. Ltd. (Beijing, China) were performed with a 3.0 T GE Signa Excite. All the animal experiments were approved by the Tianjin Medical University Animal Care and Use Committee. The mouse was anaesthetized by 4% chloral hydrate (40 mg/kg) and maintained in a small animal coil. Then it was scanned before and after the injection of Fe_3O_4@HA@Tf NPs in PBS (24 mg

Fe/kg) via the tail vein at different time points. The T_2-weighted MR images were acquired with following parameters: T_2 propeller sequence, slice thickness of 2 mm, slice spacing of 0.5 mm, TR/TE of 2932/141 ms, FOV of 8×8 cm and matrix of 256×160.

2.7 MR imaging of tumor model *in vivo*

Female Balb/c nude mice (22-25 g) were obtained from Beijing HFK Bioscience Co. Ltd. (Beijing, China). The tumor models were established by the subcutaneous planting of 2×10^6 Hela cells in the inguinal region of the nude mice. After 2-3 weeks, when tumor volume reached about 0.8-1.2 cm^3, the mice were selected for the following use. Similar to the MR imaging of normal model *in vivo*, Fe_3O_4@HA@Tf NPs in PBS (24 mg Fe/kg) was injected through the tail vein into the anaesthetized nude mice with 4% chloral hydrate (40 mg/kg). MR scanning was managed before and after the intravenous administration of the nanoparticles. The T_2-weighted MR images before and after injection at different time points were obtained with the same parameters as mentioned in the normal model. As a control, Fe_3O_4@PEG NPs were applied to the MR imaging of tumor model *in vivo* in the same way of Fe_3O_4@HA@Tf NPs.

2.8 Metabolism of Fe_3O_4@HA@Tf NPs *in vivo*

The metabolism of Fe_3O_4@HA@Tf NPs *in vivo* was evaluated via following procedures. After intravenous injection of Fe_3O_4@HA@Tf NPs in PBS (24 mg Fe/kg), mice were sacrificed at different time points (1, 7 and 30 days, n=3). Then the related metabolic organs (heart, liver, spleen, lung and kidney) were extracted. Mice without administration of nanoparticles were used as control (n=3). After digestion in aqua regia for 48 hours, samples were filtrated through 0.22 μm film and analyzed by AAS to determinate the content of Fe.

2.9 Biochemical analysis *in vivo*

To explore the physiological influences of Fe_3O_4@HA@Tf NPs *in vivo*, the changes of body weight and biochemical indicators in mice were measured at different time points after the intravenous administration of of Fe_3O_4@HA@Tf NPs in PBS (24 mg Fe/kg). After intravenous injection, mice (n=3) were weighed and extracted blood at specific time points (1, 7 and 30 days). Mice without injection of nanoparticles were used as control (n=3). The biochemical indicators of the blood samples, including total protein (TP), albumin (ALB), globulin (GLB), alanine aminotransferase (ALT), aspartate aminotransferase (AST), gamma glutamyl transaminase (GGT), creatinine (CREA) and urea were analyzed in clinical laboratory in Tianjin Medical University General Hospital.

3. Results and discussion

3.1 Synthesis and characterizations of Fe_3O_4@HA@Tf NPs

Fe_3O_4@HA NPs were synthesized using HA as a template via a one-pot co-precipitation method at room temperature. The XRD pattern of acquired Fe_3O_4@HA NPs can be easily indexed to cubic structure of Fe_3O_4 (Fig. 1a). Compared with other reported Fe_3O_4@HA NPs via post-modification method,[36, 37] the bioactivity of HA was possibly preserved at the greatest extent due to the facile procedure and mild condition. In order to further improve targeting ability, the prepared Fe_3O_4@HA NPs were modified with Tf. Tf was conjugated to Fe_3O_4@HA NPs at room temperature by using coupling agents (EDC and NHS). The presence of HA in the Fe_3O_4@HA NPs and Fe_3O_4@HA@Tf NPs was confirmed by the FT-IR spectra. As shown in Fig. S1, the characteristic absorption band at 900-1200 cm^{-1} is assigned to the C-O vibration of the carbohydrate chain of HA. The successful modification and quantification of Tf was confirmed via Bradford assay (Fig. S2†).[38] According to the result of Bradford assay and TGA (Fig. S3†), it can be calculated that there were 1.97% Tf (w/w) and 3.93% HA (w/w) in the prepared Fe_3O_4@HA@Tf NPs. The vacuum-dried Fe_3O_4@HA@Tf NPs contained 49.95% Fe (w/w), which was determinated by AAS. The above results adequately proved that both HA and Tf were successfully modified on the Fe_3O_4 NPs.

The HRTEM image of Fe_3O_4@HA@Tf NPs showed a round-like geometry with an average size of 5.8 nm (Fig. 1b, S4†). Compared with the HRTEM image of Fe_3O_4@HA NPs (Fig. S5†), there was no obvious changes in the shape and size of nanoparticles during the modification of Tf. The hydrodynamic size of Fe_3O_4@HA@Tf NPs acquired from DLS was 57.4 nm. Zeta potential of the proposed nanoparticles was -37.1 mV, which ensured the excellent colloidal stability of the nanoprobe. Both appropriate hydrodynamic size and good colloidal stability greatly facilitated the further biological applications.

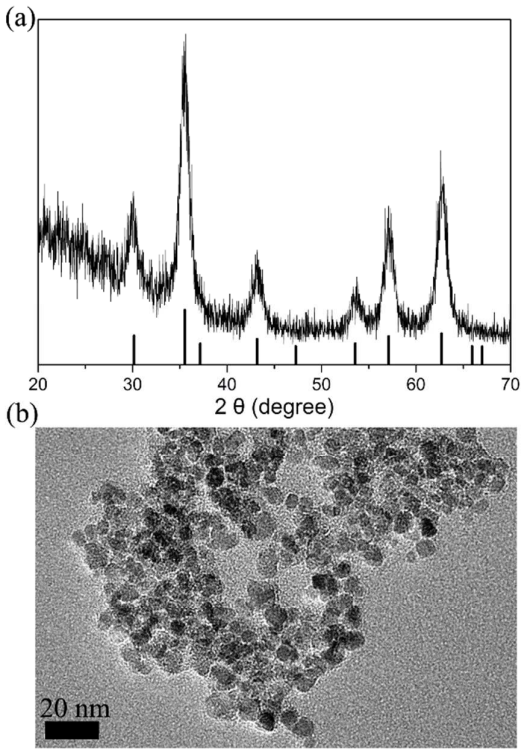

Fig. 1 (a) XRD pattern of Fe_3O_4@HA NPs. (b) HRTEM image of Fe_3O_4@HA@Tf NPs.

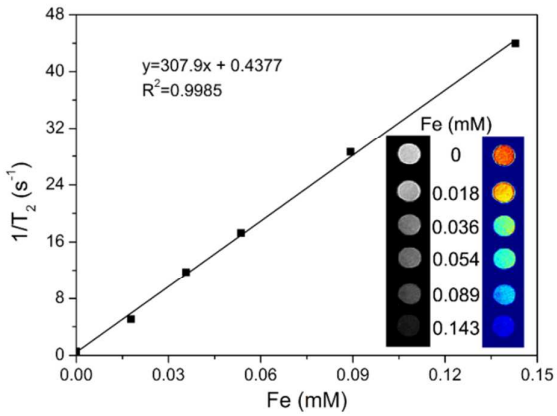

Fig. 2 Linear fitting of $1/T_2$ of Fe_3O_4@HA@Tf NPs in water, and insets were T_2-weighted MR images at the Fe concentration of 0, 0.018, 0.036, 0.054, 0.089 and 0.143 mM, respectively.

The T_2 relaxivity (r_2) value of Fe_3O_4@HA@Tf NPs calculated as the slope of the fitting curve of $1/T_2$ (s^{-1}) against Fe concentration (mM) was 307.9 $mM^{-1}s^{-1}$, which was much higher than the commercial T_2-weighted contrast agent Feridex (120 $mM^{-1}s^{-1}$ Fe)(Fig. 2).[23] It was obvious that the T_2-weighted MR signal intensity decreased with the increase of Fe concentration. Briefly, the Fe_3O_4@HA@Tf NPs exhibited great potential in contrast enhanced T_2-weighted MR imaging with high r_2 value and Fe concentration-dependent sensitivity.

3.2 *In vitro* cytotoxicity assay

The cytotoxicity of the nanoprobe was estimated via the cellular MTT assay with Hela cells. As shown in Fig. 3a, different concentrations of Fe_3O_4@HA@Tf NPs ranging from 25 to 250 μg/mL lead to negligible decrease in viability of Hela cells compared with the corresponding PBS control. Even at the concentration of 250 μg/mL, higher than the concentrations of most reported Fe_3O_4-based nanoparticles,[39, 40] the nanoprobes showed negligible influence in cell viability (cell viability >90%). No obvious cytotoxicity at the concentration up to 250 μg/mL ensured the biosafety for further in vivo MR imaging applications.

3.3 *In vitro* targeted cellular uptake test

Targeted cellular uptake test was performed to investigate whether the dual-targeting nanoprobes have more efficient targeting ability compared with single-targeting and non-targeting nanoparticles, and to illustrate the targeting ability derived from the dual interactions between targeting ligands and receptors. The receptor-blocked assay was used to establish the patterns of single receptor and none receptor. The AAS results of groups with different treatments (Fig. 3b) demonstrated that unblocked Hela cells internalized much more nanoparticles than single-blocked (CD44 or TfR-blocked) and dual-blocked (CD44 & TfR-blocked) cells at the nanoprobe concentration of 50 μg/mL as well as 100 μg/mL. It was evident that nanoparticles co-modified with dual-targeting ligands (HA and Tf) could attach more Hela cells compared with single-targeting or none-targeting nanoparticles. It was worth mentioning that the dual-blocked cells incubated with

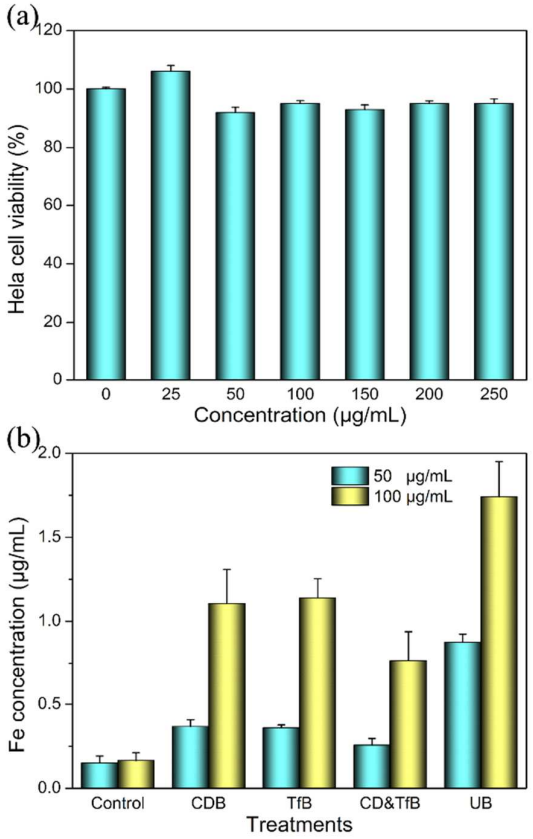

Fig. 3 (a) MTT cell viability of Hela cells after incubation with Fe_3O_4@HA@Tf NPs at different concentrations for 24 h. Cells treated with PBS were regarded as control group. (b) Cellular uptake results of Fe_3O_4@HA@Tf NPs at two concentrations (50 and 100 μg/mL) with different treatments, n=3. CDB, TfB, UB and CD&TfB meant CD44-blocked, TfR-blocked, unblocked and CD44&TfR-blocked treatments, respectively.

nanoparticles internalized more nanoparticles than the corresponding PBS control group. This was probably due to the passive transportation as a result of the higher concentration of nanoparticles outside of cells than that inside of cells, particularly at the concentration of 100 μg/mL. Such forceful targeting ability of Fe_3O_4@HA@Tf NPs in vitro ensured their potential for the application of the tumor-targeted imaging *in vivo*.

3.4 MR imaging of normal model *in vivo*

Before application in tumor-targeted MR imaging, we first applied this dual-targeting nanoparticles in normal model to evaluate the contrast effects in different organs *in vivo*. After rapid intravenous administration of the nanoparticles, the mouse was scanned via T_2-weighted MR imaging. The images (Fig. 4) showed that the liver of the mouse became black at 10 minutes post-injection of the nanoprobes, which was probably resulted from the rapid phagocytosis of the mononuclear phagocyte system (MPS).[24, 41] The massive accumulation of Fe_3O_4@HA@Tf NPs in liver induced obvious decrease of signal intensity, and the presented 'black liver' was in agreement

with previous reports.[42, 43] In the meantime, the signal intensity of kidney showed a temporary decrease but recovered in 90 min. The signal intensity of urine in the urinary bladder didn't descend, so it could be inferred that the excretion of nanoparticles through urinary system was negligible. In order to investigate the metabolism of nanoparticles in organs especially in liver for a long time, MR scan of the mouse at 7 days, 14 days and 30 days post-injection of nanoprobes were performed. It could be found that the signal intensity of liver recovered a lot at 14th day after injection and got practically full recovery after 30 days post-injection of the nanoparticles. It could be concluded that the metabolism of nanoparticles via the MPS was a relatively long process. Furthermore, biodistribution of Fe_3O_4@HA@Tf NPs in main organs (heart, liver, spleen, lung and kidney) after intravenous administration of the nanoprobe *in vivo* was evaluated by AAS. The results (Fig. S6†) confirmed that nanoparticles accumulated mainly in liver and spleen but with negligible residual in heart, lung and kidney. The impressive increase of Fe in liver and spleen occurred at 1 day post-injection of the nanoprobes. Then the nanoprobes were gradually metabolized from these two organs, which was approximately accordant with the MR images.

3.5 MR imaging of tumor model *in vivo*

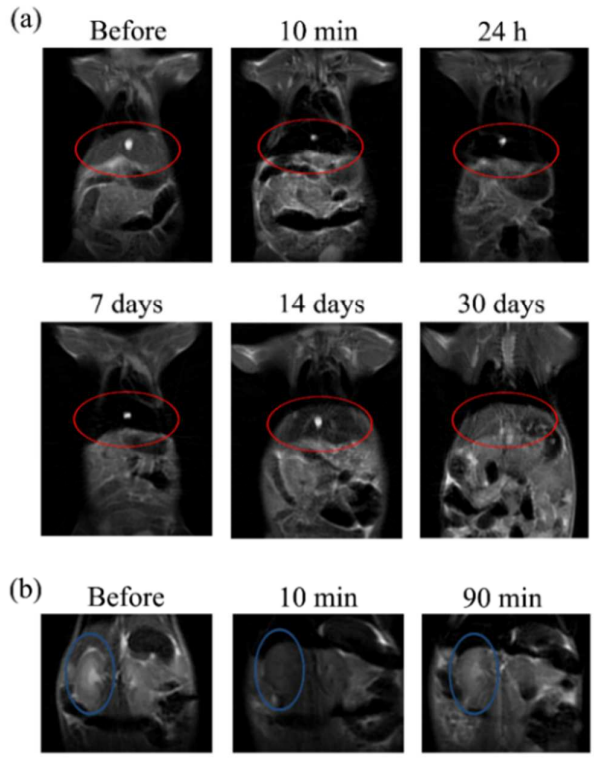

Fig. 4 T_2-weighted MR images (a, b) of normal mouse before and after intravenous administration of Fe_3O_4@HA@Tf NPs in PBS (24 mg Fe/kg) at different time points. The region with red cycle was liver (a). The region with blue cycle was kidney (b).

Obvious targeting effect in cellular uptake assay encouraged us to apply this dual-targeting nanoprobe to the diagnosis of tumors *in vivo*. As shown in Fig. 5, the signal intensity of tumor site gradually decreased in the course of time after intravenous injection of the nanoprobes. At about 1.5 hours post-injection of the nanoparticles, the signal intensity in tumor site fell to minimum (49.1% of the initial value), which resulted from dual-targeting ligands mediated specific interaction based on HA-CD44 and Tf-TfR. The signal intensity in the tumor site reached the minimum in a relatively short time, which indicated the high efficiency of the dual-targeting nanoprobes for tumor-targeted MR imaging. At 2.5 hours post-injection of nanoprobes, the MR signal in the region of tumor started to recover. Another 1.5 hours later, MR signal recovered to about 80% value of the tumor site before the administration of nanoparticles (Fig. S7†), which indicated the fact the nanoparticles underwent further metabolism process, thus resulting in the decrease of distribution in the tumor site. In the contrast, the MR signal intensity of tumor site only decreased a little (about 5%) in the course of time after administration of Fe_3O_4@PEG NPs (Fig. S7†, S8†), which was probably due to the well-known EPR effect. The obvious signal decrease in tumor site caused by Fe_3O_4@HA@Tf NPs reveals that the active targeting resulting from the dual-targeting functionalization of Fe_3O_4 NPs plays a more important role in the signal decrease of tumor site *in vivo* besides the passive targeting caused by the EPR effect. The success *in vivo* tumor-targeted MR imaging demonstrated the proposed dual-targeting nanoprobes could be used as a high specific and sensitive T_2 contrast agent for tumor-targeted MR imaging with high efficiency.

3.6 Biochemical analysis *in vivo*

Side effects of nanoprobes caused by nonspecific accumulation in MPS have been the focus attention for the applications of nanomaterials *in vivo*.[17] In this research, the experimental results revealed that the Fe_3O_4@HA@Tf NPs were mostly detained in liver, spleen and temporally stayed in kidney. Herein, biochemical indicators in mice at different time points after injection of Fe_3O_4@HA@Tf NPs through the tail vein were evaluated strictly to estimate the toxicity on those organs. As shown in Fig. 6, six typical indicators of liver function (TP, ALB, GLB, ALT, AST, GGT) and two vital biomarkers of kidney function (UREA, CREA) at 1, 7 and 30 days post-injection of the nanoprobe all exhibited no significant differences in comparison with control group. In addition, the mice with administration of Fe_3O_4@HA@Tf NPs showed no obvious loss of body weight in 30 days when compared with control group (Fig. S9†). In conclusion, no obvious toxicity on liver and kidney in the mice treated with Fe_3O_4@HA@Tf NPs in PBS at the dosage of 24 mg Fe/kg, which potently revealed the good biocompatibility of the nanoprobes *in vivo*.

4. Conclusion

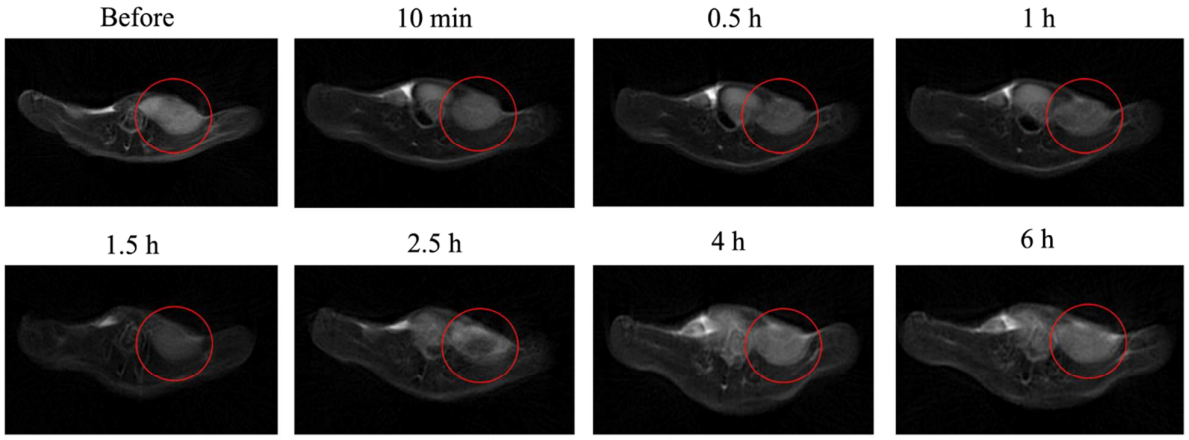

Fig. 5 T_2-weighted MR images of tumor-bearing mouse before and after intravenous administration of Fe_3O_4@HA@Tf NPs in PBS (24 mg Fe/kg) at different time points. The region with red cycle was tumor site.

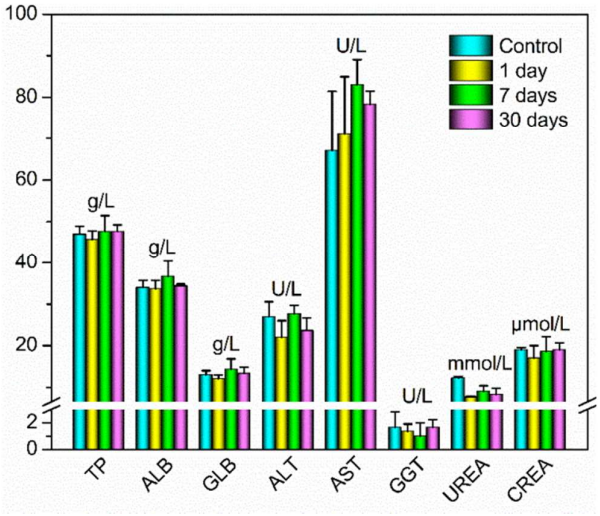

Fig. 6 Diverse biochemical markers of mice at different time points (1, 7, 30 days) after intravenous administration of Fe_3O_4@HA@Tf NPs in PBS (24 mg Fe/kg). Mice without treatments of the nanoprobe were regarded as control group, n=3.

To sum up, we employed bio-safe HA and Tf to co-modify the non-toxic Fe_3O_4 NPs to obtain a dual-targeting Fe_3O_4@HA@Tf NPs, which possess the advantages of dual-targeting ability, excellent biocompatibility, facile synthesis procedure and mild condition. Low cytotoxicity and excellent biocompatibility of the nanoprobe were confirmed by the cell viability assay, intravital metabolism and biochemical analysis. The uptake test of Hela cells and MR imaging of tumor-bearing mice exhibited the desirable tumor-targeting ability of the dual-targeting nanoparticles. More important, the developed nanoplatform provides a novel strategy based on integrating dual-targeting strategy and selection of human-inherent elements and molecules as raw materials for the fabrication of high sensitive and biocompatible nanoplatform for clinical tumor-targeted imaging *in vivo*.

Acknowledgements

This work was supported by the National Natural Science Foundation of China (Grants 21405112, 21435001, 21305103), China Postdoctoral Science Foundation (Grants 2014M550146).

References

1. A. Jemal, F. Bray, M. M. Center, J. Ferlay, E. Ward and D. Forman, *CA Cancer J. Clin.*, 2011, **61**, 69.
2. Y. Matsumura and H. Maeda, *Cancer Res.*, 1986, **46**, 6387.
3. J. Y. Yhee, S. Lee and K. Kim, *Nanoscale*, 2014, **6**, 13383.
4. Z. Cheng, A. Al Zaki, J. Z. Hui, V. R. Muzykantov and A. Tsourkas, *Science*, 2012, **338**, 903.
5. M. K. Yu, J. Park and S. Jon, *Theranostics*, 2012, **2**, 3.
6. S. Oliveira, R. Heukers, J. Sornkom, R. J. Kok and P. M. P. v. B. E. Henegouwen, *J. Control. Release*, 2013, **172**, 607.
7. R. Toy, L. Bauer, C. Hoimes, K. B. Ghaghada and E. Karathanasis, *Adv. Drug Deliver. Rev.*, 2014, **76**, 79.
8. E. Kluza, D. W. J. van der Schaft, P. A. I. Hautvast, W. J. M. Mulder, K. H. Mayo, A. W. Griffioen, G. J. Strijkers and K. Nicolay, *Nano Lett.*, 2010, **10**, 52.
9. X. Zheng, D. Xing, F. Zhou, B. Wu and W. R. Chen, *Mol. Pharm.*, 2011, **8**, 447.
10. W. Pan, H. Yang, T. Zhang, Y. Li, N. Li and B. Tang, *Anal. Chem.*, 2013, **85**, 6930.
11. H. Kobayashi and P. L. Choyke, *Acc. Chem. Res.*, 2011, **44**, 83.
12. G.-L. Davies, I. Kramberger and J. J. Davis, *Chem. Commun.*, 2013, **49**, 9704.
13. X. Wang, C.-X. Yang, J.-T. Chen and X.-P. Yan, *Anal. Chem.*, 2014, **86**, 3263.
14. N. Lewinski, V. Colvin and R. Drezek, *Small*, 2008, **4**, 26.
15. J. Ai, E. Biazar, M. Jafarpour, M. Montazeri, A. Majdi, S. Aminifard, M. Zafari, H. R. Akbari and H. G. Rad, *Int. J. Nanomed.*, 2011, **6**, 1117.
16. A. Kunzmann, B. Andersson, T. Thurnherr, H. Krug, A. Scheynius and B. Fadeel, *Biochim. Biophys. Acta.*, 2011, **1810**, 361.
17. S. Sharifi, S. Behzadi, S. Laurent, M. L. Forrest, P. Stroeve and M. Mahmoudi, *Chem. Soc. Rev.*, 2012, **41**, 2323.
18. M. A. Hahn, A. K. Singh, P. Sharma, S. C. Brown and B. M. Moudgil, *Anal. Bioanal. Chem.*, 2011, **399**, 3.

19. S. J. Soenen, P. Rivera-Gil, J.-M. Montenegro, W. J. Parak, S. C. De Smedt and K. Braeckmans, *Nano Today*, 2011, **6**, 446.
20. Y. Teow, P. V. Asharani, M. P. Hande and S. Valiyaveettil, *Chem. Commun.*, 2011, **47**, 7025.
21. X. Li, L. Wang, Y. Fan, Q. Feng and F.-z. Cui, *J. Nanomater.*, 2012, 548389.
22. J. Li, X. Chang, X. Chen, Z. Gu, F. Zhao, Z. Chai and Y. Zhao, *Biotechnol. Adv.*, 2014, **32**, 727.
23. N. Lee and T. Hyeon, *Chem. Soc. Rev.*, 2012, **41**, 2575.
24. L. H. Reddy, J. L. Arias, J. Nicolas and P. Couvreur, *Chem. Rev.*, 2012, **112**, 5818.
25. J. Gallo, N. J. Long and E. O. Aboagye, *Chem. Soc. Rev.*, 2013, **42**, 7816.
26. M. Mahmoudi, H. Hofmann, B. Rothen-Rutishauser and A. Petri-Fink, *Chem. Rev.*, 2012, **112**, 2323.
27. G. Liu, J. Gao, H. Ai and X. Chen, *Small*, 2013, **9**, 1533.
28. L. Yang, H. Kuang, W. Zhang, Z. P. Aguilar, Y. Xiong, W. Lai, H. Xu and H. Wei, *Nanoscale*, 2014, **7**, 625.
29. J. P. M. Almeida, A. L. Chen, A. Foster and R. Drezek, *Nanomedicine*, 2011, **6**, 815.
30. B. P. Toole, *Nat. Rev. Cancer*, 2004, **4**, 528.
31. G. Saravanakumar, V. G. Deepagan, R. Jayakumar and J. H. Park, *J. Biomed. Nanotechnol.*, 2014, **10**, 17.
32. S. Tortorella and T. C. Karagiannis, *J. Membrane. Biol.*, 2014, **247**, 291.
33. K. Y. Choi, H. Chung, K. H. Min, H. Y. Yoon, K. Kim, J. H. Park, I. C. Kwon and S. Y. Jeong, *Biomaterials*, 2010, **31**, 106.
34. K. Y. Choi, K. H. Min, H. Y. Yoon, K. Kim, J. H. Park, I. C. Kwon, K. Choi and S. Y. Jeong, *Biomaterials*, 2011, **32**, 1880.
35. A. Moore, L. Josephson, R. M. Bhorade, J. P. Basilion and R. Weissleder, *Radiology*, 2001, **221**, 244.
36. M. Kamat, K. El-Boubbou, D. C. Zhu, T. Lansdell, X. W. Lu, W. Li and X. F. Huang, *Bioconjugate. Chem.*, 2010, **21**, 2128.
37. J. Li, Y. He, W. Sun, Y. Luo, H. Cai, Y. Pan, M. Shen, J. Xia and X. Shi, *Biomaterials*, 2014, **35**, 3666.
38. M. M. Bradford, *Anal. Biochem.*, 1976, **72**, 248.
39. H. Yang, Y. Zhuang, Y. Sun, A. Dai, X. Shi, D. Wu, F. Li, H. Hu and S. Yang, *Biomaterials*, 2011, **32**, 4584.
40. J. H. Lee, M. J. Jung, Y. H. Hwang, Y. J. Lee, S. Lee, D. Y. Lee and H. Shin, *Biomaterials*, 2012, **33**, 4861.
41. B. Wang, X. He, Z. Zhang, Y. Zhao and W. Feng, *Acc. Chem. Res.*, 2013, **46**, 761.
42. P. Reimer and T. Balzer, *Eur. Radiol.*, 2003, **13**, 1266.
43. H. B. Na, I. C. Song and T. Hyeon, *Adv. Mater.*, 2009, **21**, 2133.